

6. Cho, I.; Lee, J.-Y. *J. Polym. Sci., Polym. Lett. Ed.* **1983**, *21*, 389.
7. Florianczyk, T.; Sullivan, C.; Janovic, Z.; Vogl, O. *Polym. Bull.* **1981**, *5*, 521.
8. Xi, F.; Bassett, W.; Vogl, O. *J. Polym. Sci.: Polym. Chem. Ed.* **1983**, *21*, 891.
9. Williams, J. K.; Wiley, D. W.; McKusick, B. C. *J. Am. Chem. Soc.* **1962**, *84*, 2210.
10. Hall, Jr. H. K.; Ykman, P. *J. Am. Chem. Soc.* **1975**, *97*, 800.
11. Hall, Jr. H. K.; Rasoul, H. A. A.; Gillard, M.; Abdelkader, M.; Nogue, P.; Sentman, R. C. *Tetrahedron Lett.* **1982**, *23*, 603.
12. Hall, Jr. H. K.; Padias, A. B. *Acc. Chem. Res.* **1990**, *23*, 3.
13. Kresel, M.; Garbratski, U.; Kohn, D. H. *J. Polym. Sci., Part A* **1964**, *2*, 105.
14. Gilath, A.; Ronel, S. H.; Shmueli, M.; Kohn, D. H. *J. Appl. Polym. Sci.* **1970**, *14*, 1491.
15. Ronel, S. H.; Shmueli, M.; Kohn, D. H. *J. Polym. Sci., A-1* **1969**, *7*, 2209.
16. Lieberon, A.; Kohn, D. H. *J. Polym. Sci., Polym. Chem. Ed.* **1974**, *12*, 2435.
17. Kharas, G.; Kohn, D. H. *J. Polym. Sci., Polym. Chem. Ed.* **1983**, *21*, 1457.
18. Kharas, G.; Kohn, D. H. *J. Polym. Sci., Polym. Chem. Ed.* **1984**, *22*, 583.
19. Angelorici, M. M.; Kohn, D. H. *J. Appl. Polym. Sci.* **1990**, *40*, 485.
20. Tanaka, H. *Trends Polym. Sci.* **1993**, *1*, 361.
21. Tanaka, H. *Trends Polym. Sci.* **1996**, *4*, 106.
22. Lee, J.-Y. *Polym. Bull.* **1996**, *36*, 525.
23. Moore, A. H. F. *Org. Syn. Coll. Vol. 4* **1963**, 84.
24. Corson, B. B.; Stoughton, R. W. *J. Am. Chem. Soc.* **1928**, *50*, 2825.
25. Lee, J.-Y.; Lee, H.-J.; Kim, M.-Y. *Polym. Bull.* **1997**, *38*, 27.

## Solid-State $^{51}\text{V}$ NMR and Infrared Spectroscopic Study of Vanadium Oxide Supported on $\text{ZrO}_2\text{-WO}_3$

Jong Rack Sohn\*, Man Ho Lee, Im Ja Doh<sup>†</sup>, and Young Il Pae<sup>†</sup>

*Department of Industrial Chemistry, Engineering College, Kyungpook National University, Taegu 702-701, Korea*

<sup>†</sup>*Department of Chemistry, University of Ulsan, Ulsan 680-749, Korea*

*Received April 15, 1998*

Vanadium oxide catalyst supported on  $\text{ZrO}_2\text{-WO}_3$  was prepared by adding the  $\text{Zr}(\text{OH})_4$  powder into a mixed aqueous solution of ammonium metavanadate and ammonium metatungstate followed by drying and calcining at high temperatures. The characterization of prepared catalysts was performed using solid-state  $^{51}\text{V}$  NMR and FTIR. In the case of calcination temperature at 773 K, for the samples containing low loading  $\text{V}_2\text{O}_5$  below 18 wt % vanadium oxide was in a highly dispersed state, while for samples containing high loading  $\text{V}_2\text{O}_5$  equal to or above 18 wt % vanadium oxide was well crystallized due to the  $\text{V}_2\text{O}_5$  loading exceeding the formation of monolayer on the surface of  $\text{ZrO}_2\text{-WO}_3$ . The  $\text{ZrV}_2\text{O}_7$  compound was formed through the reaction of  $\text{V}_2\text{O}_5$  and  $\text{ZrO}_2$  at 873 K and the compound decomposed into  $\text{V}_2\text{O}_5$  and  $\text{ZrO}_2$  at 1073 K, which were confirmed by FTIR and  $^{51}\text{V}$  NMR.

### Introduction

Vanadium oxides are widely used as catalysts in oxidation reactions, e.g., the oxidation of sulfur dioxide, carbon monoxide, and hydrocarbons.<sup>1-4</sup> These systems have also been found to be effective catalysts for the oxidation of methanol to methylformate.<sup>5,6</sup> Much research has been done to understand the nature of active sites, the surface structure of catalysts as well as the role played by the promoter of the supported catalysts, using infrared (IR), X-ray diffraction (XRD), electron spin resonance (E.S.R) and Raman spectroscopy.<sup>6-9</sup> So far, silica, titania, zirconia and alumina<sup>10-17</sup> have been commonly employed as the vanadium oxide supports, and comparatively very few works have been reported for bi-

nary oxide,  $\text{ZrO}_2\text{-WO}_3$  as the support for vanadium oxide.

It is well known that the dispersion and the structural features of supported species can strongly depend on the support. Structure and other physicochemical properties of supported metal oxides are considered to be in different states compared with bulk metal oxides because of their interaction with the supports. Solid-state nuclear magnetic resonance (NMR) methods represent a novel and promising approach to these systems. Since only the local environment of a nucleus under study is probed by NMR, this method is well suited for the structural analysis of disordered systems such as the two-dimensional surface vanadium oxide phases which is of particular interest in the present study. In addition to the structural information provided by NMR methods, the direct proportionality of the signal intensity to the number of contributing nuclei makes NMR be useful

\*Author to whom correspondence should be addressed.

for quantitative studies. In the present investigation, the techniques of solid-state  $^{51}\text{V}$  NMR and Fourier transform infrared (FTIR) have been utilized to characterize a series of  $\text{V}_2\text{O}_5$  samples supported on  $\text{ZrO}_2\text{-WO}_3$  with various vanadia loadings.

## Experimental

**Catalyst Preparation.** Precipitate of  $\text{Zr}(\text{OH})_4$  was obtained by adding aqueous ammonia slowly into an aqueous solution of zirconium oxychloride at room temperature with stirring until the pH of mother liquor reached about 8. The precipitate thus obtained was washed thoroughly with distilled water until chloride ion was not detected, and was dried at room temperature for 12 h. The dried precipitate was powdered below 100 mesh.

The catalysts containing various vanadium oxide content were prepared by adding the  $\text{Zr}(\text{OH})_4$  powder into a mixed aqueous solution of ammonium metavanadate ( $\text{NH}_4\text{VO}_3$ ) and ammonium metatungstate [ $(\text{NH}_4)_6(\text{H}_2\text{W}_{12}\text{O}_{40})\cdot n\text{H}_2\text{O}$ ] followed by drying and calcining at high temperatures for 1.5h. This series of catalysts are denoted by their weight percentage of  $\text{V}_2\text{O}_5$ , where the content of  $\text{WO}_3$  in all catalysts was fixed as 15 wt %. For example, 3- $\text{V}_2\text{O}_5/\text{ZrO}_2\text{-WO}_3$  indicates the catalyst containing 3 wt %  $\text{V}_2\text{O}_5$ .

**Characterization.** FTIR absorption spectra of  $\text{V}_2\text{O}_5/\text{ZrO}_2\text{-WO}_3$  powders were measured by the KBr disk method over the range 1200-400  $\text{cm}^{-1}$ . The samples for the KBr disk method were prepared by grinding a mixture of the catalyst and KBr powders in an agate mortar and pressing them in the usual way. FTIR spectra of ammonia adsorbed on the catalyst were obtained in a heatable gas cell at room temperature using a Mattson Model GL 6030E spectrophotometer. The self-supporting catalyst wafers contained about 9  $\text{mg}/\text{cm}^2$ . Prior to obtaining the spectra the samples were heated under vacuum at 673-773 K for 1.5 h.

$^{51}\text{V}$  NMR spectra were measured by a Varian Unity Inova 300 spectrometer with a static magnetic field strength of 7.05 T. Larmor frequency was 78.89 MHz. The ordinary single pulse sequence was used, in which the pulse width was set at 2.8 s and the acquisition time was 0.026 s. The spectral width was 500 kHz. The number of scans was varied from 400 to 4,000, depending on the concentration of vanadium. The signal was acquired from the time point 4s after the end of the pulse. The sample was static, and its temperature was ambient (294 K). The spectra were expressed with the signal of  $\text{VOCl}_3$  being 0 ppm, and the higher frequency shift from the standard was positive. Practically, solid  $\text{NH}_4\text{VO}_3$  (-571.5 ppm) was used as the second external reference.<sup>18</sup>

## Results and Discussion

**Infrared Spectra.** Figure 1 shows IR spectra of  $\text{V}_2\text{O}_5/\text{ZrO}_2\text{-WO}_3$  catalysts with various content calcined at 773 K for 1.5 h. Although with samples below 18 wt % of  $\text{V}_2\text{O}_5$  the definite peaks were not observed, the absorption bands at 1022 and 820  $\text{cm}^{-1}$  appeared for 18- $\text{V}_2\text{O}_5/\text{ZrO}_2\text{-WO}_3$ , 23- $\text{V}_2\text{O}_5/\text{ZrO}_2\text{-WO}_3$ , 28- $\text{V}_2\text{O}_5/\text{ZrO}_2\text{-WO}_3$  and pure  $\text{V}_2\text{O}_5$  containing high  $\text{V}_2\text{O}_5$  content. The band at 1022  $\text{cm}^{-1}$  is assigned to the V=O stretching vibration, while that at 820  $\text{cm}^{-1}$  is

attributable to the coupled vibration between V=O and to V-O-V.<sup>19</sup> Generally, the IR band of V=O in crystalline  $\text{V}_2\text{O}_5$  shows at 1020-1025  $\text{cm}^{-1}$  and the Raman band at 995  $\text{cm}^{-1}$ .<sup>2,20</sup> The intensity of the V=O absorption gradually decreased with increasing  $\text{ZrO}_2$  content, although the band position did not change. As shown in Figure 1, the catalysts at vanadia loadings below 18 wt % gave no absorption bands due to crystalline  $\text{V}_2\text{O}_5$ . This observation suggests that vanadium oxide below 18 wt % is in a highly dispersed state. It is reported that  $\text{V}_2\text{O}_5$  loading exceeding the formation of monolayer on the surface of  $\text{ZrO}_2$  is well crystallized and observed in the spectra of IR and  $^{51}\text{V}$  solid state NMR.<sup>21</sup>

As shown in Figure 1, for 4- $\text{V}_2\text{O}_5/\text{ZrO}_2\text{-WO}_3$  and 12- $\text{V}_2\text{O}_5/\text{ZrO}_2\text{-WO}_3$  calcined at 773 K the crystalline  $\text{V}_2\text{O}_5$  was not observed in their IR spectra, suggesting the monolayer dispersion of  $\text{V}_2\text{O}_5$  on the surface  $\text{ZrO}_2\text{-WO}_3$  as the amorphous phase. However, it is necessary to examine the formation of crystalline  $\text{V}_2\text{O}_5$  as a function of calcination temperature. Variations of IR spectra against calcination temperature for 4- $\text{V}_2\text{O}_5/\text{ZrO}_2\text{-WO}_3$  and 12- $\text{V}_2\text{O}_5/\text{ZrO}_2\text{-WO}_3$  are shown in Figures 2 and 3, respectively. For both catalysts, there are no V=O stretching bands at 1022  $\text{cm}^{-1}$  from 673 to 973 K of the calcination temperature, indicating no formation of crystalline  $\text{V}_2\text{O}_5$ . However, as shown in Figures 2 and 3, V=O stretching bands due to crystalline  $\text{V}_2\text{O}_5$  at 1073 K and 1173 K appeared at 1022  $\text{cm}^{-1}$  together with lattice vibration

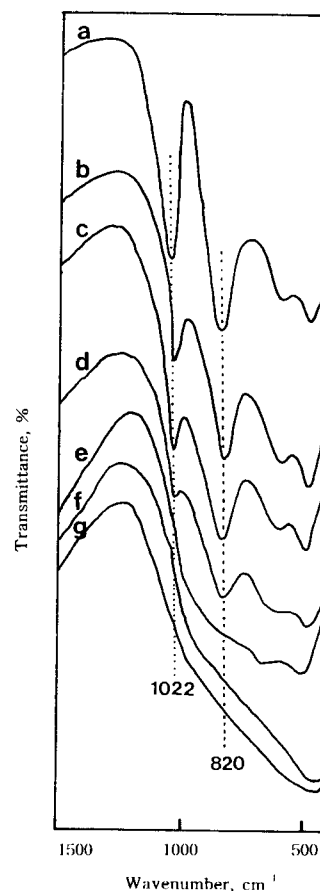


**Figure 1.** Infrared spectra of catalysts calcined at 773 K: (a)  $\text{V}_2\text{O}_5$ , (b) 28- $\text{V}_2\text{O}_5/\text{ZrO}_2\text{-WO}_3$ , (c) 23- $\text{V}_2\text{O}_5/\text{ZrO}_2\text{-WO}_3$ , (d) 18- $\text{V}_2\text{O}_5/\text{ZrO}_2\text{-WO}_3$ , (e) 12- $\text{V}_2\text{O}_5/\text{ZrO}_2\text{-WO}_3$ , (f) 8- $\text{V}_2\text{O}_5/\text{ZrO}_2\text{-WO}_3$ , (g) 4- $\text{V}_2\text{O}_5/\text{ZrO}_2\text{-WO}_3$ .

bands of  $V_2O_5$  and  $WO_3$  below  $900\text{ cm}^{-1}$ .<sup>22,23</sup> The formation of crystalline  $V_2O_5$  above  $1073\text{ K}$  can be explained in terms of the decomposition of  $ZrV_2O_7$  compound which was formed through the reaction of  $V_2O_5$  and  $ZrO_2$  at  $873\text{--}973\text{ K}$ . In this work, on X-ray diffraction patterns the cubic phase of  $ZrV_2O_7$  was observed in the samples calcined at  $873\text{ K}$  and for sample calcined at  $1173\text{ K}$  the  $ZrV_2O_7$  phase disappeared due to the decomposition of  $ZrV_2O_7$ , leaving the  $V_2O_5$  phase and the monoclinic phase of  $ZrO_2$ . These results are in good agreement with those of  $^{51}\text{V}$  solid state NMR described later. In fact, it is known that the formation of  $ZrV_2O_7$  from  $V_2O_5$  and  $ZrO_2$  occurs at  $873\text{ K}$  of calcination temperature and the  $ZrV_2O_7$  decomposes into  $ZrO_2$  and  $V_2O_5$  at  $1073\text{ K}$ .<sup>21,24</sup>

Figure 4 shows IR spectra of  $28\text{-V}_2\text{O}_5/\text{ZrO}_2\text{-WO}_3$  catalysts calcined at  $673\text{--}1073\text{ K}$  for  $1.5\text{ h}$ . Unlike  $4\text{-V}_2\text{O}_5/\text{ZrO}_2\text{-WO}_3$  and  $12\text{-V}_2\text{O}_5/\text{ZrO}_2\text{-WO}_3$  catalysts, for  $28\text{-V}_2\text{O}_5/\text{ZrO}_2\text{-WO}_3$  crystalline  $V_2O_5$  appeared at lower calcination temperature from  $673\text{ K}$  to  $873\text{ K}$  and consequently  $\text{V}=\text{O}$  stretching band was observed at  $1022\text{ cm}^{-1}$ . This is because  $V_2O_5$  loading exceeding the formation of monolayer on the surface of  $ZrO_2$  is well crystallized.<sup>21</sup> However, at  $973\text{ K}$  all  $V_2O_5$  reacted with  $ZrO_2$  and changed into  $ZrV_2O_7$  so that  $\text{V}=\text{O}$  stretching at  $1022\text{ cm}^{-1}$  disappeared completely, as shown in Figure 4. At  $1073\text{ K}$  of calcination temperature some of  $ZrV_2O_7$  decomposed into  $V_2O_5$  and  $ZrO_2$  and then  $\text{V}=\text{O}$  stretching band due to the crystalline  $V_2O_5$  was again observed at  $1022\text{ cm}^{-1}$ . These results are in good agreement with those of  $^{51}\text{V}$  solid state NMR.

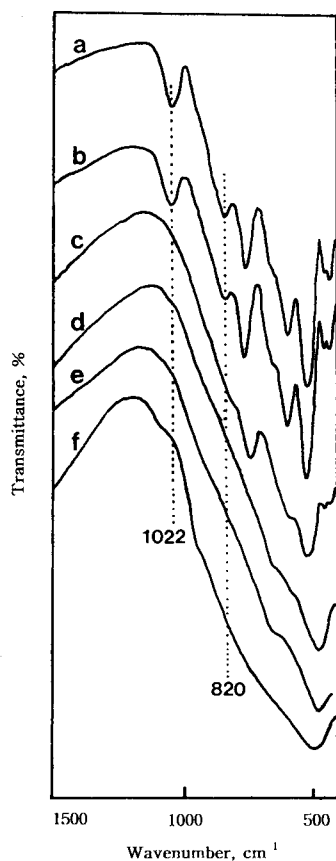


**Figure 2.** Infrared spectra of  $4\text{-V}_2\text{O}_5/\text{ZrO}_2\text{-WO}_3$  calcined at (a)  $1173\text{ K}$ , (b)  $1073\text{ K}$ , (c)  $973\text{ K}$ , (d)  $873\text{ K}$ , (e)  $773\text{ K}$ , and (f)  $673\text{ K}$ .

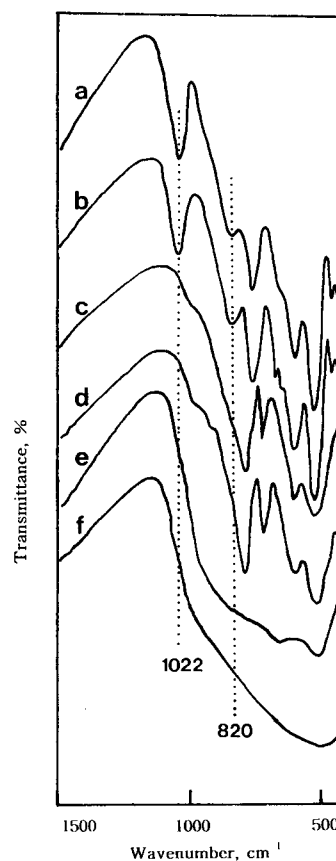


**Figure 3.** Infrared spectra of  $12\text{-V}_2\text{O}_5/\text{ZrO}_2\text{-WO}_3$  calcined at (a)  $1173\text{ K}$ , (b)  $1073\text{ K}$ , (c)  $973\text{ K}$ , (d)  $873\text{ K}$ , (e)  $773\text{ K}$ , and (f)  $673\text{ K}$ .

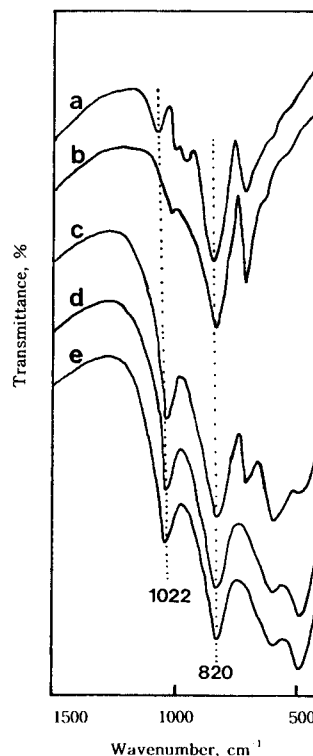


**Figure 4.** Infrared spectra of  $28\text{-V}_2\text{O}_5/\text{ZrO}_2\text{-WO}_3$  calcined at (a)  $1073\text{ K}$ , (b)  $973\text{ K}$ , (c)  $873\text{ K}$ , (d)  $773\text{ K}$ , and (e)  $673\text{ K}$ .

**$^{51}\text{V}$  Solid State NMR Spectra.** Solid state NMR methods represent a novel and promising approach to vanadium oxide catalytic materials. The solid state  $^{51}\text{V}$  NMR spectra of  $\text{V}_2\text{O}_5/\text{ZrO}_2\text{-WO}_3$  catalysts calcined at 773 K are shown in Figure 5. There are three types of signals in the spectra of catalysts with varying intensities depending on  $\text{V}_2\text{O}_5$  content. At the low loadings up to 12 wt%  $\text{V}_2\text{O}_5$  a shoulder at about 260 ppm and the intense peak at 590-650 ppm are observed. The former is assigned to the surface vanadium-oxygen structures surrounded by a distorted octahedron of oxygen atoms, while the latter is attributed to the tetrahedral vanadium-oxygen structures.<sup>25,26</sup>

However, the surface vanadium oxide structure is remarkably dependent on the metal oxide support material. Vanadium oxide on  $\text{TiO}_2$  (anatase) displays the highest tendency to be 6-coordinated at low surface coverages, while in the case of  $\gamma\text{-Al}_2\text{O}_3$  a tetrahedral surface vanadium species is the favored.<sup>25</sup> As shown in Figure 5, at low vanadium loading on  $\text{ZrO}_2\text{-WO}_3$  a tetrahedral vanadium species is exclusively dominant compared with an octahedral species. In general, it is known that low surface coverages favor a tetrahedral coordination of vanadium oxide, while at higher surface coverages vanadium oxide becomes increasingly octahedral-coordinated. As shown in Figure 5, the peak shapes for the vanadium species on  $\text{ZrO}_2\text{-WO}_3$  are narrower and more symmetric compared to those of vanadium species on  $\text{TiO}_2$  or  $\gamma\text{-Al}_2\text{O}_3$  reported by other reporters.<sup>25,26</sup> It seems likely that the different physical and chemical properties of  $\text{ZrO}_2\text{-WO}_3$  from those of  $\text{TiO}_2$  or  $\gamma\text{-Al}_2\text{O}_3$  affect the symmetry of the surface vanadium-oxygen structures.

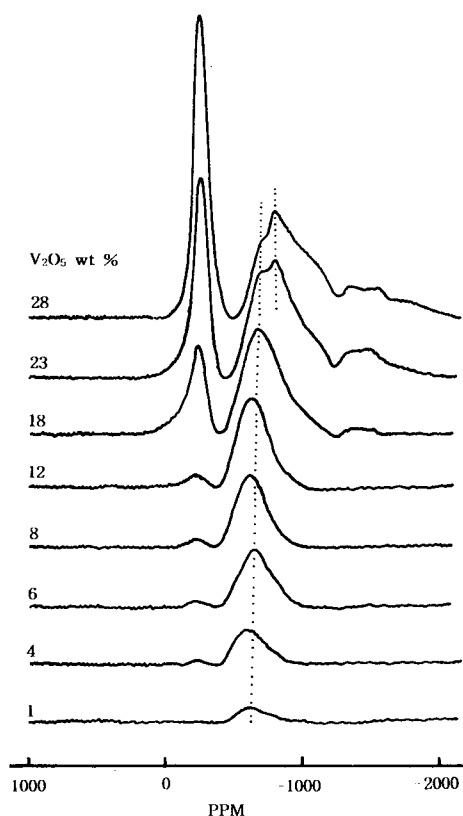


**Figure 5.** Solid state  $^{51}\text{V}$  NMR spectra of  $\text{V}_2\text{O}_5/\text{ZrO}_2\text{-WO}_3$  catalysts calcined at 773 K.

Increasing the  $\text{V}_2\text{O}_5$  content on the  $\text{ZrO}_2\text{-WO}_3$  surface changes the shape of the spectrum to a rather intense and sharp peak at about 300 ppm ( $\delta_{\perp}$ ) and a broad low-intensity peak at about 1400 ppm ( $\delta_{\parallel}$ ), which are due to the crystalline  $\text{V}_2\text{O}_5$  of square pyramid coordination.<sup>25</sup> These observations of crystalline  $\text{V}_2\text{O}_5$  for samples containing high  $\text{V}_2\text{O}_5$  content above 12 wt % are in good agreement with the results of the IR spectra in Figure 1. Namely, this is because  $\text{V}_2\text{O}_5$  loading exceeding the formation of monolayer on the surface of  $\text{ZrO}_2\text{-WO}_3$  is well crystallized.<sup>21</sup> Moreover, the increase in  $\text{V}_2\text{O}_5$  content resulted appearance of additional signals with a peak in the range from 810 to 840 ppm. The intensity of the signal increases with increase in  $\text{V}_2\text{O}_5$  loading. Different peak positions normally indicate the differences of the spectral parameters and are observed due to different local environments of vanadium nuclei.<sup>25-29</sup> Thus species at -590~-650 ppm and -810~-840 ppm can be attributed to two types of tetrahedral vanadium complexes with different oxygen environments. Namely, the signals at -590~-650 ppm can be attributed to the surface vanadium complexes containing OH groups or water molecules in their coordination sphere,<sup>26</sup> because the evacuation treatment decreases the intensities remarkably. On the other hand, the signals at -810~-840 ppm are due to the surface tetrahedral vanadium complexes which do not contain OH groups or adsorbed water molecules.

It is necessary to examine the effect of calcination temperature on the surface vanadium oxide structure. The spectra of 4- $\text{V}_2\text{O}_5/\text{ZrO}_2\text{-WO}_3$  and 12- $\text{V}_2\text{O}_5/\text{ZrO}_2\text{-WO}_3$  containing lower vanadium oxide content and calcined at various temperatures are shown in Figures 6 and 7, respectively. The shape of the spectrum is very different depending on the cal-

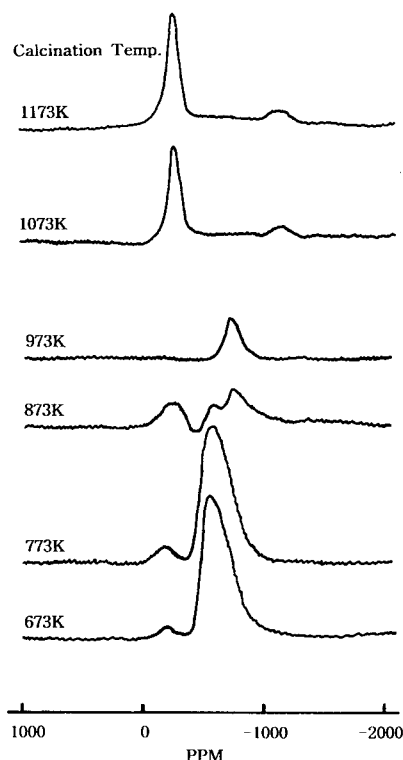


**Figure 6.** Solid state  $^{51}\text{V}$  NMR spectra of 4- $\text{V}_2\text{O}_5/\text{ZrO}_2\text{-WO}_3$  calcined at different temperatures.

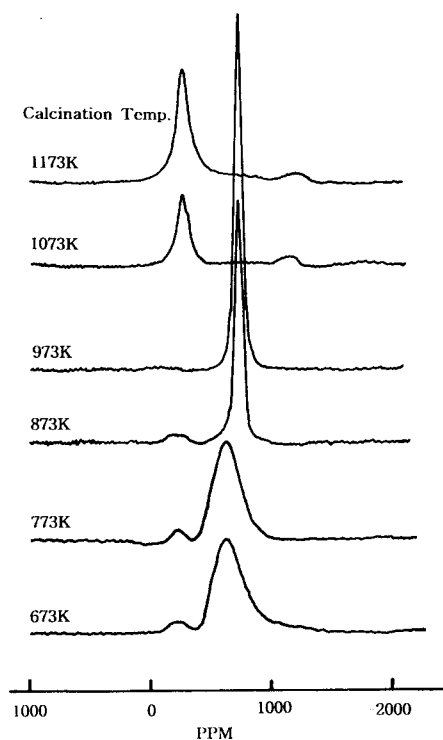


**Figure 7.** Solid state  $^{51}\text{V}$  NMR spectra of  $12\text{-V}_2\text{O}_5/\text{ZrO}_2\text{-WO}_3$  calcined at different temperatures.

calcination temperature. For both samples calcined at lower temperatures (673–773 K), two peaks at about 260 ppm and  $-590\sim-650$  ppm due to the octahedral and tetrahedral vanadium-oxygen structures are shown, indicating the monolayer dispersion of  $\text{V}_2\text{O}_5$  on the  $\text{ZrO}_2$  surface, in good agreement with the results of IR spectra of Figures 2 and 3. However, for samples calcined at 873 K, in addition to the above two peaks a sharp peak at 800 ppm due to crystalline  $\text{ZrV}_2\text{O}_7$  appeared, indicating the formation of a new compound from  $\text{V}_2\text{O}_5$  and  $\text{ZrO}_2$  at high calcination temperature. For samples calcined at 873–1073 K X-ray diffraction patterns of  $\text{ZrV}_2\text{O}_7$  were observed. Roozeboom *et al.* reported the formation of  $\text{ZrV}_2\text{O}_7$  from  $\text{V}_2\text{O}_5$  and  $\text{ZrO}_2$  at 873 K of calcination temperature.<sup>24</sup> At 973 K of calcination temperature only a peak at 802 ppm due to the  $\text{ZrV}_2\text{O}_7$  phase appeared, saying that most of  $\text{V}_2\text{O}_5$  on the surface of  $\text{ZrO}_2\text{-WO}_3$  was consumed to form the  $\text{ZrV}_2\text{O}_7$  compound. However, at 1073–1173 K of calcination temperature we can observe only the peaks of crystalline  $\text{V}_2\text{O}_5$  at 290 ppm and about 1200 ppm, indicating the decomposition of  $\text{ZrV}_2\text{O}_7$ . These results are in good agreement with those of IR spectra in Figures 2 and 3.

The spectra of  $28\text{-V}_2\text{O}_5/\text{ZrO}_2\text{-WO}_3$  containing higher vanadium oxide content than monolayer loading and calcined at various temperatures are shown in Figure 8. Unlike  $4\text{-V}_2\text{O}_5/\text{ZrO}_2\text{-WO}_3$  and  $12\text{-V}_2\text{O}_5/\text{ZrO}_2\text{-WO}_3$  catalysts, for  $28\text{-V}_2\text{O}_5/\text{ZrO}_2\text{-WO}_3$  calcined even at lower temperatures (673–773 K) a sharp peak due to crystalline  $\text{V}_2\text{O}_5$  appeared at 290 ppm together with peaks at 670 and 870 ppm due to the tetrahedral surface species. However, for sample calcined at 873 K, in addition to a peak at 300 ppm due to crystalline  $\text{V}_2\text{O}_5$  a sharp peak at 800 ppm due to  $\text{ZrV}_2\text{O}_7$  compound appeared. As shown in Figure 8, the peak intensity of  $\text{ZrV}_2\text{O}_7$

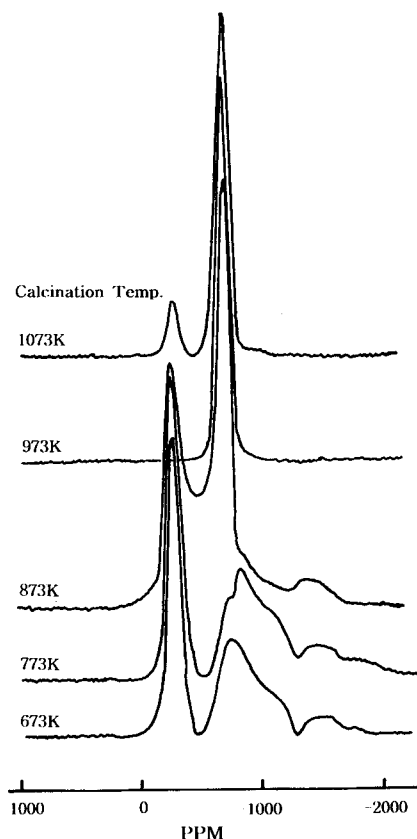


**Figure 8.** Solid state  $^{51}\text{V}$  NMR spectra of  $28\text{-V}_2\text{O}_5/\text{ZrO}_2\text{-WO}_3$  calcined at different temperatures.

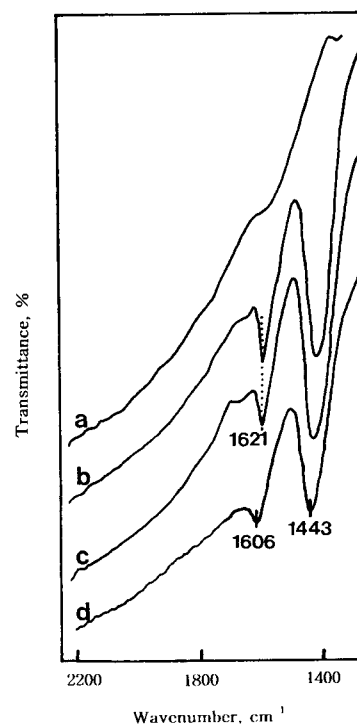


**Figure 9.** Infrared spectra of  $\text{NH}_3$  adsorbed on  $4\text{-V}_2\text{O}_5/\text{ZrO}_2\text{-WO}_3$  calcined at 973 K.: (a) background of  $4\text{-V}_2\text{O}_5/\text{ZrO}_2\text{-WO}_3$  evacuated at 673 K for 1 h, (b)  $\text{NH}_3$  (20 torr) adsorbed on (a), (c) b sample evacuated at 298 K for 5 min, and (d) c sample evacuated at 503 K for 0.5 h.

increased with increase in calcination temperature, consuming the content of crystalline V<sub>2</sub>O<sub>5</sub>. Consequently, at 973 K of calcination temperature only a peak due to the ZrV<sub>2</sub>O<sub>7</sub> phase appeared at 800 ppm. At 1073 K of calcination temperature a sharp peak of crystalline V<sub>2</sub>O<sub>5</sub> at 290 ppm due to the decomposition of ZrV<sub>2</sub>O<sub>7</sub> was again observed. However, unlike 4-V<sub>2</sub>O<sub>5</sub>/ZrO<sub>2</sub>-WO<sub>3</sub> and 12-V<sub>2</sub>O<sub>5</sub>/ZrO<sub>2</sub>-WO<sub>3</sub>, for 28-V<sub>2</sub>O<sub>5</sub>/ZrO<sub>2</sub>-WO<sub>3</sub> the ZrV<sub>2</sub>O<sub>7</sub> compound was not decomposed completely at 1073 K, leaving some of ZrV<sub>2</sub>O<sub>7</sub>. It seems likely that it is very difficult for all ZrV<sub>2</sub>O<sub>7</sub> to decompose for 1.5 h because large amount of ZrV<sub>2</sub>O<sub>7</sub> was formed in the case of 28-V<sub>2</sub>O<sub>5</sub>/ZrO<sub>2</sub>-WO<sub>3</sub>.

**Acidic Properties.** The acid strength of the catalysts was examined by a color change method, using Hammett indicator<sup>30</sup> in dried sulfuric chloride. Since it was very difficult to observe the color of indicators adsorbed on catalysts of high vanadium oxide content, a low percentage of vanadium content (1 wt%) was used in this experiment. ZrO<sub>2</sub> evacuated at 773 K for 1 h has an acid strength  $H_0 \leq +1.5$ , while 1-V<sub>2</sub>O<sub>5</sub>/ZrO<sub>2</sub> was estimated to have a  $H_0 \leq -11.35$ , indicating the formation of new acid sites stronger than those of oxide components. The acid strength of 1-V<sub>2</sub>O<sub>5</sub>/ZrO<sub>2</sub>-WO<sub>3</sub> was also found to be  $H_0 \leq -14.5$ . Acids stronger than  $H_0 \leq -11.93$ , which corresponds to the acid strength of 100% H<sub>2</sub>SO<sub>4</sub>, are superacids.<sup>31</sup> Consequently, V<sub>2</sub>O<sub>5</sub>/ZrO<sub>2</sub>-WO<sub>3</sub> catalysts would be solid superacids. The superacidic property is attributed to the double bond nature of the W=O in the complex formed by the interaction of ZrO<sub>2</sub> with WO<sub>3</sub>.<sup>32</sup> That is, the acid strength of samples modified with WO<sub>3</sub> becomes stronger by the inductive effect of W=O in the complex.

Infrared spectroscopic studies of ammonia adsorbed on solid surfaces have made it possible to distinguish between Brønsted and Lewis acid sites.<sup>33,34</sup> Figure 9 shows the IR spectra of ammonia adsorbed on 4-V<sub>2</sub>O<sub>5</sub>/ZrO<sub>2</sub>-WO<sub>3</sub> calcined at 973 K and evacuated at 673 K for 1 h. For 4-V<sub>2</sub>O<sub>5</sub>/ZrO<sub>2</sub>-WO<sub>3</sub> the bands at 1443 are the characteristic peaks of ammonium ion, which are formed on the Brønsted acid sites and the other set of adsorption peaks at 1621-1606 cm<sup>-1</sup> is contributed by ammonia coordinately bonded to Lewis acid sites,<sup>33,34</sup> indicating the presence of both Brønsted and Lewis acid sites. The band shift of adsorbed ammonia from 1621 cm<sup>-1</sup> to 1606 cm<sup>-1</sup> after evacuation at 503 K for 0.5 h is due to the removal of ammonia adsorbed on weak acid sites or physically adsorbed ammonia. Other samples having different vanadium content also showed the presence of both Lewis and Brønsted acids. Therefore, these V<sub>2</sub>O<sub>5</sub>/ZrO<sub>2</sub>-WO<sub>3</sub> samples can be used as catalysts for Lewis or Brønsted acid catalysis.

## Conclusions

This paper has shown that a combination of FTIR and <sup>51</sup>V solid-state NMR can be used to perform the characterization of V<sub>2</sub>O<sub>5</sub> catalysts supported on ZrO<sub>2</sub>-WO<sub>3</sub>. On the basis of results of FTIR and solid state <sup>51</sup>V NMR, at low calcination temperature of 773 K vanadium oxide up to 12 wt% was well dispersed on the surface of ZrO<sub>2</sub>-WO<sub>3</sub>. However, high V<sub>2</sub>O<sub>5</sub> loading (equal to or above 18 wt%) exceeding the formation of monolayer on the surface of ZrO<sub>2</sub>-WO<sub>3</sub> was well crystallized. The ZrV<sub>2</sub>O<sub>7</sub> compound

was formed through the reaction of V<sub>2</sub>O<sub>5</sub> and ZrO<sub>2</sub> at 873 K and the compound decomposed into V<sub>2</sub>O<sub>5</sub> and ZrO<sub>2</sub> at 1073 K, which were observed in the spectra of FTIR and solid state <sup>51</sup>V NMR. Infrared spectroscopic studies of ammonia adsorbed on V<sub>2</sub>O<sub>5</sub>/ZrO<sub>2</sub>-WO<sub>3</sub> catalysts showed the presence of both Lewis and Brønsted acids.

**Acknowledgment.** This paper was supported by the Korea Science and Engineering Foundation through the Research Center for Catalytic Technology at Pohang University of Science and Technology.

## References

1. Nakagawa, Y.; Ono, T.; Miyata, H.; Kubokawa, Y. *J. Chem. Soc., Faraday Trans. 1* **1983**, 79, 2929.
2. Miyata, H.; Kohno, M.; Ono, T.; Ohno, T.; Hatayama, F. *J. Chem. Soc., Faraday Trans. 1* **1989**, 85, 3663.
3. Mars, P.; Van Krevelen, D. W. *Oxidations Carried Out by Means of Vanadium Oxide Catalysts, Spec. Suppl. Chem. Eng.* **1954**, 3, 41.
4. Sachtler, W. M. H. *Catal. Rev.* **1970**, 4, 27.
5. Forzatti, P.; Tronoconi, E.; Busca, G.; Titarell, P. *Catal. Today* **1987**, 1, 209.
6. Busca, G.; Elmi, A. S.; Forzatti, P. *J. Phys. Chem.* **1987**, 91, 5263.
7. Elmi, A. S.; Tronoconi, E.; Cristiani, C.; Martin, J. P. G.; Forzatti, P. *Ind. Eng. Chem. Res.* **1989**, 84, 237.
8. Miyata, H.; Fujii, K.; Ono, T.; Kubokawa, Y.; Ohno, T.; Hatayama, F. *J. Chem. Soc., Faraday Trans. 1* **1987**, 83, 675.
9. Cavani, F.; Centi, G.; Foresti, E.; Trifiro, F. *J. Chem. Soc., Faraday Trans. 1* **1988**, 84, 237.
10. Hayata, F.; Ohno, T.; Maruoka, T.; Miyata, H. *J. Chem. Soc., Faraday Trans.* **1991**, 87, 2629.
11. Arco, M. del; Holgado, M. J.; Martin, C.; Rives, V. *Langmuir* **1990**, 6, 801.
12. Centi, G.; Pinelli, D.; Trifiro, F.; Ghossoub, D.; Gugelton, M.; Gengembre, L. *J. Catal.* **1991**, 130, 238.
13. Inomata, M.; Mori, K.; Miyamoto, A.; Murakami, Y. *J. Phys. Chem.* **1983**, 87, 761.
14. Scharf, U.; Schraml Marth, M.; Wokaun, A.; Baiker, A. *J. Chem. Soc., Faraday Trans.* **1991**, 87, 3299.
15. Scharf, U.; Schraml-Marth, M.; Wokaun, A.; Baiker, A. *J. Chem. Soc., Faraday Trans.* **1991**, 87, 3299.
16. Miyata, H.; Kohno, M.; Ono, T.; Ohno, T.; Hatayama, F. *J. Mol. Catal.* **1990**, 63, 181.
17. Sohn, J. R.; Park, M. Y.; Pae, Y. I. *Bull. Korean Chem. Soc.* **1996**, 17, 274.
18. Hayashi, S.; Hayamizu, K. *Bull. Chem. Soc. Jpn.* **1990**, 63, 961.
19. Mori, K.; Miyamoto, A.; Murakami, Y. *J. Chem. Soc., Faraday Trans.* **1987**, 83, 3303.
20. Bjorklund, R. B.; Odenbrand, C. U. I.; Brandin, J. G. M.; Anderson, L. A. H.; Liedberg, B. *J. Catal.* **1989**, 119, 187.
21. Sohn, J. R.; Cho, S. G.; Pae, Y. I.; Hayashi, S. *J. Catal.* **1996**, 159, 170.
22. Inomata, M.; Miyamoto, A.; Murakami, Y. *J. Catal.* **1980**, 62, 140.
23. Highfield, J. G.; Moffat, J. B. *J. Catal.* **1984**, 88, 177.
24. Roozeboom, F.; Mittelmeljer-Hazeleger, M. C.; Moulijn, J. A.; Medema, J.; de Beer, U. H. J.; Gelling,

- P. J. *J. Phys. Chem.* **1980**, *84*, 2783.  
 25. Eckert, H.; wachs, I. E. *J. Phys. Chem.* **1989**, *93*, 6796.  
 26. Reddy, B. M.; Reddy, E. P.; Srinivas, S. T.; Mastikhin, V. M.; Nosov, N. V.; Lapina, O. B. *J. Phys. Chem.* **1992**, *96*, 7076  
 27. Le Costumer, L. R.; Taouk, B.; Le Meur, M.; Payen, E.; Guelton, M.; Grimblot, J. *J. Phys. Chem.* **1988**, *92*, 1230.  
 28. Narsimha, K.; Reddy, B. M.; Rao, P. K.; Mastikhin, V. M. *J. Phys. Chem.* **1990**, *94*, 7336.  
 29. Sobalik, Z.; Lapina, O. B.; Novgorodova, O. N.; Mastikhin, V. M. *Appl. Catal.* **1990**, *63*, 191.

30. Sohn, J. R.; Lee, S. Y. *Appl. Catal. A: General* **1997**, *164*, 127.  
 31. Olah, F. G. A.; Prakash, G. K. S.; Sommer, J. *Science* **1979**, *206*, 13.  
 32. Bernhole, J.; Horseley, J. A.; Murrell, L. L.; Sherman, L. G.; Soled, S. *J. Phys. Chem.* **1987**, *97*, 1526.  
 33. Basila, M. R.; Kantner, T. R. *J. Phys. Chem.* **1967**, *71*, 467.  
 34. Satsuma, A.; Hattori, A.; Mizutani, K.; Furuta, A.; Miyamoto, A.; Hattori, T.; Murakami, Y. *J. Phys. Chem.* **1988**, *92*, 6052.

## Stereocontrolled Preparation of 2,6-Disubstituted 4-Methylenetetrahydropyrans by Lewis Acid Promoted Allylsilane-Acetal Cyclization

Tae Myung Sung, Woo Young Kwak, and Kyung-Tae Kang\*

Department of Chemistry, Chemistry Institute for Functional Materials,  
Pusan National University, Pusan 609-735, Korea

Received April 23, 1998

The Lewis acid mediated intramolecular additions of allylsilanes to acetal substrates are described. Excellent regio- and diastereoselectivity are achieved by boron trifluoride promoted cyclization of allylsilane-acetals **5** and **8** derived from hydroxy allylsilanes **3**. Cyclizations occur in moderate to high yields, providing direct routes to *cis*-2,6-disubstituted 4-methylenetetrahydropyrans **6** and **9**.

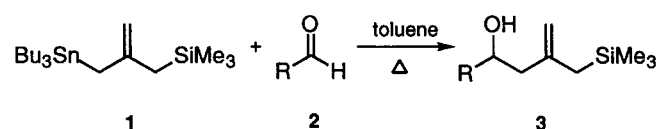
### Introduction

Tetrahydropyrans are important structural units in a variety of biologically active natural products.<sup>1</sup> Consequently, there are many efficient methods for the preparation of the six-membered oxacycles.<sup>2</sup> However, these methods were not useful for the straightforward synthesis of 4-methylenetetrahydropyrans because of difficult control for the regioselective formation of exomethylene moiety. 4-Methylenetetrahydropyran is a key-subunit present in the novel macrolides such as phorphoxazoles A and B,<sup>3</sup> and zampanolide<sup>4</sup> which exhibit exceedingly potent cytostatic activity against various human solid tumor cell lines.

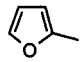
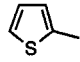
Intramolecular cyclizations of allylsilanes with an electrophile have become exceedingly useful for highly regio- and stereoselective formation of various ring compounds.<sup>5</sup> Indeed, Marko *et al.* reported that the intramolecular silyl-modified Sakurai (ISMS) reaction allowed the construction of the 4-methylenetetrahydropyrans, however, 2,6-disubstituted derivatives were not found.<sup>6</sup>

In continuation of our studies on exploring synthetic application of bimetallic reagents containing silicon and tin atoms,<sup>7</sup> we found that 3-stannyl-2-(silylmethyl)propene **1** reacted smoothly with aldehydes in refluxing toluene even without any catalytic activation to give hydroxy allylsilanes **3** in good yields.<sup>8</sup>

In this paper we present our investigation of the regioselective formation of a variety of 2,6-disubstituted 4-methylenetetrahydropyrans by Lewis acid promoted cyclization of allylsilanes having an acetal group derived from



**Table 1.** Preparation of allylsilane-acetals **5** and their cyclizations to 4-methylenetetrahydropyrans **6**

Entry	Allylsilane-acetal <b>5</b>		Tetrahydropyran <b>6</b> Yield (%) <sup>d</sup>
	R	Yield (%) <sup>a</sup> (Ratio of Diastereomers) <sup>b,c</sup>	
a	Ph	92 (70:30)	59 41 (SnCl <sub>4</sub> ) <sup>g</sup> <5 (ZnCl <sub>2</sub> ) <sup>f</sup>
b	p-NO <sub>2</sub> C <sub>6</sub> H <sub>4</sub>	91 (85:15) <sup>b</sup>	80
c	p-EtO <sub>2</sub> CC <sub>6</sub> H <sub>4</sub>	95 (75:25)	57
d	<i>trans</i> -PhCH=CH	97 (70:30)	78
e		90 (60:40)	17
f		87 (80:20)	20
g	CH <sub>3</sub> CH <sub>2</sub> CH <sub>2</sub>	82 (70:30)	53

<sup>a</sup> Isolated yields. <sup>b</sup> The ratio of diastereomers was determined by <sup>1</sup>H NMR analysis. <sup>c</sup> Diastereomers were separated by chromatography (SiO<sub>2</sub>, hexane: ether=15:1) unless otherwise noted. The higher R<sub>f</sub> diastereomers were major isomers. <sup>d</sup> Reactions were carried out in dichloromethane at -78 °C with 2 equiv of BF<sub>3</sub>·OEt<sub>2</sub> unless otherwise noted. <sup>e</sup> SnCl<sub>4</sub>, 2 equiv, CH<sub>2</sub>Cl<sub>2</sub>, -78 °C. <sup>f</sup> ZnCl<sub>2</sub>, 2 equiv, CH<sub>2</sub>Cl<sub>2</sub>, -78 °C-20 °C.